

Modeling of the Starting Performance of Large Solid-Pole Synchronous Motors Using Equivalent Circuit Approach

Chunting Chris Mi¹, Yongbin Li¹, and Haran Karmaker²

¹Department of Electrical and Computer Engineering, University of Michigan, Dearborn, MI 48128 USA

²Electrical Research and Development, TECO-Westinghouse, Round Rock, TX 78681 USA

We present a method of modeling the starting performance of large solid pole synchronous motors based on an equivalent circuit approach. In this approach, the solid rotor body is assumed to have two sets of separate virtual windings. Therefore, the two-axis theory can be used for the solid pole synchronous motor. We derived parameters associated with the solid-pole, together with their transformation coefficients. We simulated the starting performance and validated the results by testing a 15 000 hp, 13.2 kV, four-pole solid-pole synchronous motor.

Index Terms—Equivalent circuit, skin effect, solid pole synchronous motor, starting performance, transformation coefficient, two-axis theory, virtual windings.

I. INTRODUCTION

LARGE MOTORS in the 10–20 MW power range are used to drive compressors, blowers, and pumps in petroleum refineries, steel mills, and power plants [1]–[6]. Large solid pole motors are a special category of large motors that are very popular in industrial systems. The solid pole is made of solid pieces of forged steel, which provides high mechanical strength for high speed rotating equipments. Compared to the traditional synchronous motors with laminated rotors, whose starting torque is developed from the damping bars on the rotor, the starting torque of solid pole motors is developed by the eddy currents induced on the surface of solid-pole shoes. It is a much more complicated process [7]. The transient performance characteristics during starting, such as starting current, torque, accelerating time, and power factor, are difficult to predict. These studies require more accurate parameters and models [8].

Finite element analysis (FEA) is often used in electric motor design to calculate the parameters and performances [9]–[13]. When used in a solid pole synchronous motor (SPSM), FEA can help to understand the transient behavior such as the starting performance. However, performing transient FEA simulation with rotor motion is still cumbersome and sometimes not feasible for industrial applications. For example, the starting performance simulation of the solid-pole synchronous prototype motor shown in Fig. 1 takes 135 h to simulate a single starting using 2-D transient FEA on a 3.4 GHz, 8 GB, dual-core, 64-bit workstation. In order to shorten the design cycle, many efforts have been focused on the modeling of motors using nonlinear magnetic circuit approach and equivalent circuit method [14]–[20]. However, most studies are focused on the laminated salient pole synchronous machines with damping windings on the rotor surface, or induction motors, not for solid-pole synchronous motors [21]–[24]. Analytical solutions were derived from magnetic field theory for round rotor solid pole motors [25]. For SPSM with salient poles, more simplifying assumptions are needed for the analytical solution.

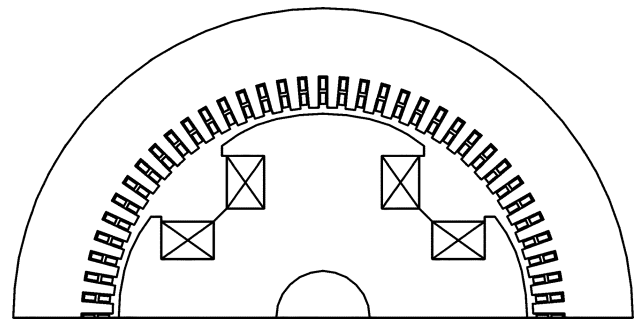


Fig. 1. Geometry model of the prototype motor. The motor is made with solid, forged steel pole. It is a four-pole motor with 72 stator slots.

TABLE I
RATED DATA OF THE PROTOTYPE

Items	Value	Unit
Rated Power	15,000	HP
Rated Voltage	13,200	V
Frequency	60	Hz
Rated speed	1,800	rpm

Based on the traditional two-axis equivalent circuit model of the salient pole synchronous motor [26], we present an improved extended equivalent circuit model for the large solid pole synchronous motor. In this model, the solid-pole body is replaced by two virtual windings, and their transformation coefficients were derived according to the operating conditions. The starting performance was simulated and validated with a 15 000 hp prototype SPSM. All these efforts indicated that the proposed model can be used to design and analyze SPSM with sufficient accuracy and significantly reduced design and analysis time.

II. TWO-AXIS MODEL AND ITS EQUIVALENT CIRCUITS

The geometry model of the prototype SPSM is shown in Fig. 1. It is a three-phase, four-pole SPSM with axial cooling ducts in the stator. The rated data of the motor is listed in Table I.

It can be seen from the geometry that a SPSM is similar to a traditional salient-pole synchronous motor, except that the rotor

Manuscript received February 19, 2009. Current version published November 18, 2009. Corresponding author: C. C. Mi (e-mail: mi@ieee.org).

Color versions of one or more of the figures in this paper are available online at <http://ieeexplore.ieee.org>.

Digital Object Identifier 10.1109/TMAG.2009.2023646

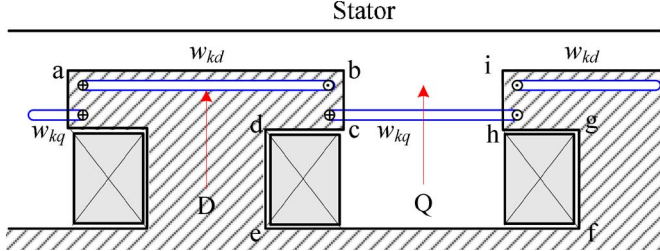


Fig. 2. Developed view of the geometry models of the solid rotor.

is made from a solid body, not from laminated steel; and there are no damping bars on the SPSM's rotor surface. Although there are no damping windings on its rotor, eddy currents are induced on the rotor surface during starting because the rotor is made from a solid metal body with high conductivity.

A SPSM is also different from a solid pole induction motor. A solid pole induction machine has a round rotor while a SPSM has a solid salient pole rotor. Therefore, solid pole induction motor theory cannot be used to analyze a SPSM.

But one can easily find that the rotor of a SPSM is similar to a laminated pole synchronous motor. The surface of the solid pole is similar to the rotor bars of laminated pole. During starting of the solid pole synchronous motor, the solid rotor surface generates eddy currents due to the rotating flux of the stator. These eddy currents are concentrated on the surface of the rotor due to skin effect, and are not symmetrical due to the rotor structure. The eddy currents can be assumed flowing in fictitious windings that represent the solid rotor that carries the eddy currents. Since the eddy currents are not symmetrical, we can assume that there are two sets of separate virtual damping windings mounted on the rotor surface, one is coupled with the d-axis and the other with the q-axis; and they are perpendicular to each other, as shown in Fig. 2. The resistance and inductance can be calculated using the properties of the solid pole material, considering the skin effect.

With the virtual windings employed, the two-axis theory used in traditional salient-pole synchronous motors [26] can be extended to the SPSM. During starting, the field winding is shorted with a discharge resistor. When the rotor speed reaches near 95% synchronous speed, the field winding is switched to a dc power supply. Therefore, the voltage equations of the stator and rotor can be written as follows:

$$\begin{cases} u_d = R_s \cdot i_d + \frac{d}{dt} \psi_d - \omega_R \cdot \psi_q \\ u_q = R_s \cdot i_q + \frac{d}{dt} \psi_q + \omega_R \cdot \psi_d \end{cases} \quad (1)$$

$$\begin{cases} 0 = (R'_{fd} + R'_s) \cdot i'_{fd} + \frac{d}{dt} \psi'_{fd}, & \text{slip} > 0.05 \\ u'_{fd} = R'_{fd} \cdot i'_{fd} + \frac{d}{dt} \psi'_{fd}, & \text{slip} \leq 0.05 \\ 0 = R'_{kd} \cdot i'_{kd} + \frac{d}{dt} \psi'_{kd} \\ 0 = R'_{kq} \cdot i'_{kq} + \frac{d}{dt} \psi'_{kq} \end{cases} \quad (2)$$

where u_d and u_q are the d-axis and q-axis voltage, respectively; R_s is the stator resistance; u'_{fd} is voltage of the field winding; i_d and i_q are d-axis and q-axis current, respectively; i'_{fd} is field winding current seen on the stator side; Ψ_d and Ψ_q are d-axis and q-axis flux linkage, respectively; ω_R is the angular speed of the rotor; R'_s is the stator resistance reflected on the rotor site;

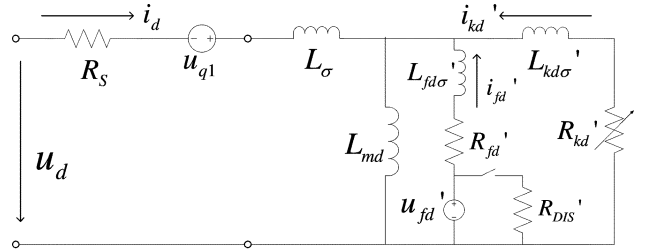


Fig. 3. Extended equivalent circuit models of the SPSM. (a) Direct axis equivalent circuit. (b) Quadrature axis equivalent circuit.

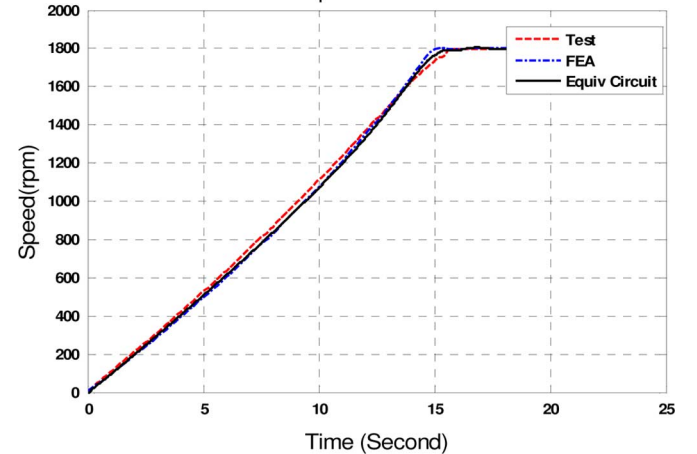


Fig. 4. Accelerating speed comparison between analytical simulation, 2-D transient FEA with motion solver simulation, and measurement.

R'_{fd} is resistance of the field winding; R'_{kd} and R'_{kq} are the resistances of virtual windings seen on the d-axis and q-axis, respectively; i'_{fd} is the excitation current of the field winding; Ψ_{kd} and Ψ_{kq} are d-axis and q-axis flux linkage of the rotor virtual winding, respectively; and i_{kd} and i_{kq} are d-axis and q-axis current of the rotor virtual winding, respectively.

The flux linkages in the above equations can be expressed as follows:

$$\begin{cases} \psi_d = L_d \cdot i_d + L_{md} \cdot (i'_{fd} + i'_{kd}) \\ \psi_q = L_q \cdot i_q + L_{mq} \cdot i'_{kq} \end{cases} \quad (3)$$

$$\begin{cases} \psi'_{fd} = L'_{fd} \cdot i'_{fd} + L_{md} \cdot (i_d + i'_{kd}) \\ \psi'_{kd} = L'_{kd} \cdot i'_{kd} + L_{md} \cdot (i_d + i'_{fd}) \\ \psi'_{kq} = L'_{kq} \cdot i'_{kq} + L_{mq} \cdot i_q \end{cases} \quad (4)$$

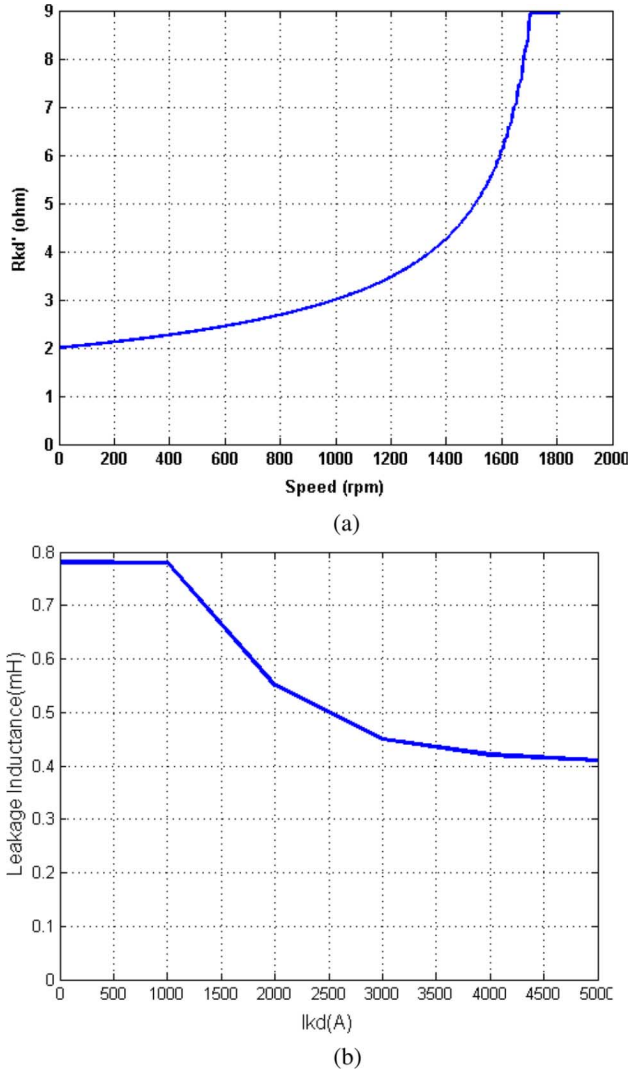


Fig. 5. Rotor resistance versus speed and inductance versus motor current derived from 2-D static FEA simulation. (a) Rotor resistance versus speed and (b) rotor leakage inductance versus current.

where L_d and L_q are the d-axis and q-axis inductance, respectively; L_{mq} is the mutual inductance; L'_{fd} is the inductance of the field winding; L'_{kd} and L'_{kq} are the leakage inductance of the rotor virtual winding, respectively

$$\begin{cases} L_d = L_\sigma + L_{md} \\ L_q = L_\sigma + L_{mq} \\ L_{kd} = L_{kd\sigma} + L_{md} \\ L_{kq} = L_{kq\sigma} + L_{mq} \\ L_{fd} = L_{fd\sigma} + L_{md} \end{cases} \quad (5)$$

where L_{md} and L_{mq} are the d- and q-axis mutual inductance, respectively; $L_{kd\sigma}$, $L_{kq\sigma}$ and $L_{fd\sigma}$ are the leakage inductance of the rotor virtual winding and field winding, respectively; and L_σ is the stator winding end-turn leakage inductance.

The equivalent circuit can be derived using (1)–(5), as shown in Fig. 3.

In Fig. 3, R'_{DIS} is the resistance of the discharge resistor. The voltage variables, u_{d1} and u_{q1} , are the induced voltages corre-

sponding to d and q-axis flux linkage, and are expressed as follows:

$$\begin{cases} u_d = \omega_R \cdot \varphi_d \\ u_q = \omega_R \cdot \varphi_q \end{cases}. \quad (6)$$

III. PARAMETER CALCULATIONS AND TRANSFORMATION COEFFICIENTS

Most parameters in the equivalent circuit can be derived from the magnetic circuit analysis [18] or FEA [27].

There is no damping winding on the rotor of solid-pole machines, and the rotor poles consist of the solid conductive bodies. Therefore, the torque in solid pole motors is developed by the eddy currents in the solid pole surface, while the torque in laminated salient pole synchronous motors is developed by the rotor pole damper winding currents. During starting, the rotor frequency varies with the rotor speed. Therefore, there will be skin effect in the solid-pole surface. The rotor resistance will vary with slip. It is assumed that the two virtual windings are covering the rotor surface with one turn; its height equals to the skin depth; and the length of the winding is the same as the actual rotor length. Then the resistors of the d and q-axis virtual windings can be described as follows:

$$\begin{cases} r_{kd} = \frac{l_r}{p \cdot \sigma \cdot l_{kd} \cdot \Delta} \\ r_{kq} = \frac{l_r}{p \cdot \sigma \cdot l_{kq} \cdot \Delta} \end{cases} \quad (7)$$

where l_r is the rotor length along the axial direction; p is number of the poles; l_{kd} and l_{kq} are the virtual windings cross section width in radial direction (refer to the model in Fig. 2); and Δ is the height of the virtual winding, which is similar to the skin effect depth. l_{kd} and l_{kq} can be calculated by

$$\begin{cases} l_{kd} = \overline{ab} \\ l_{kq} = \overline{bc} + \overline{cd} + \overline{de} + \overline{ef} + \overline{fg} + \overline{gh} + \overline{hi} \end{cases}. \quad (8)$$

The height Δ can be derived from Maxwell equations as follows:

$$\begin{cases} \text{rot } \dot{\vec{H}} = \dot{\vec{J}}; & \text{rot } \dot{\vec{E}} = \frac{\partial \vec{B}}{\partial t} \\ \dot{\vec{J}} = \frac{\dot{\vec{E}}}{\rho}; & \dot{\vec{B}} = \mu \dot{\vec{H}} \end{cases}. \quad (9)$$

Therefore

$$\frac{d^2 \dot{\vec{H}}}{dy^2} = j \frac{\omega \mu}{\rho} \cdot \dot{\vec{H}} = k^2 \cdot \dot{\vec{H}} \quad (10)$$

where

$$k = \sqrt{j \frac{\omega \mu}{\rho}} = (1+j)a. \quad (11)$$

Therefore, the depth of skin effect is

$$\begin{aligned} \Delta &= \frac{1}{a} = \sqrt{\frac{2}{\omega \cdot \mu \cdot \sigma}}, \quad \text{where } \sigma = 1/\rho \\ &\text{Or} \\ \Delta &= \sqrt{\frac{2}{\omega_r \cdot \mu \cdot \sigma}} = \sqrt{\frac{1}{\pi \cdot f_s \cdot s \cdot \mu \cdot \sigma}} \end{aligned} \quad (12)$$

where s is the rotor slip; f_s is the frequency of the power supply; μ and σ are the permeability and conductivity of the solid rotor material.

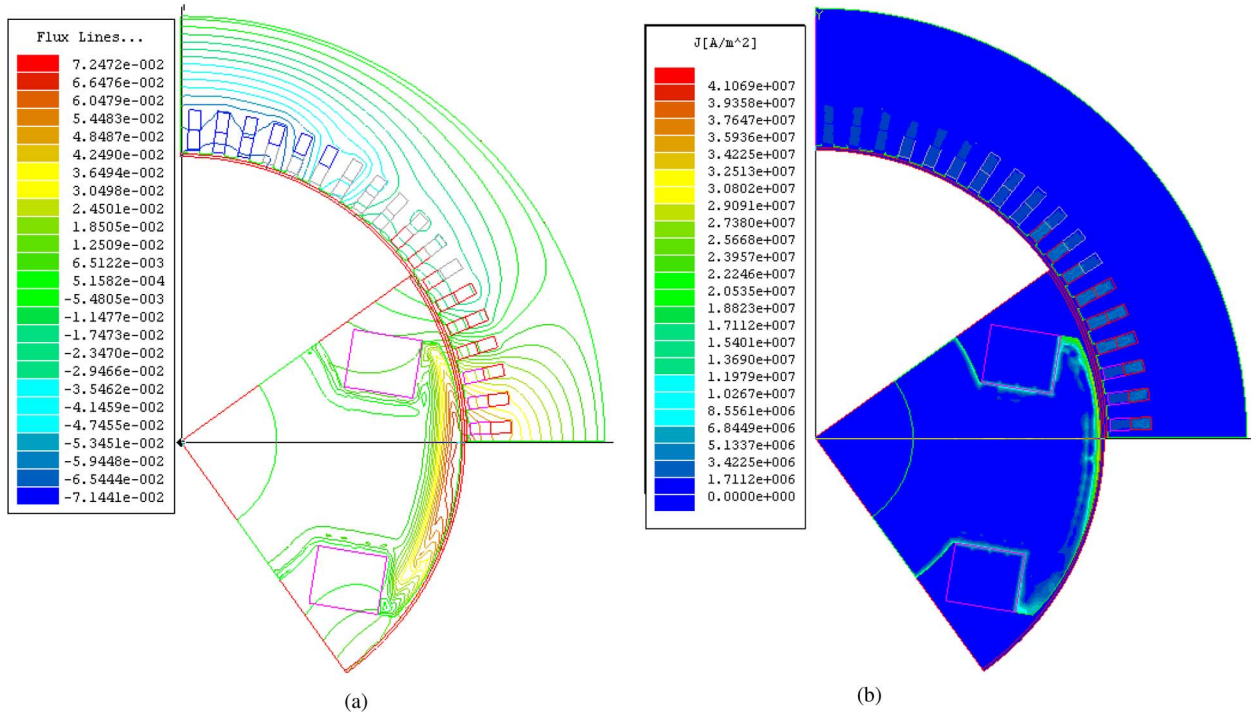


Fig. 6. Flux and current density distributions obtained from 2-D FEA. (a) Flux line distribution and (b) Eddy current distribution.

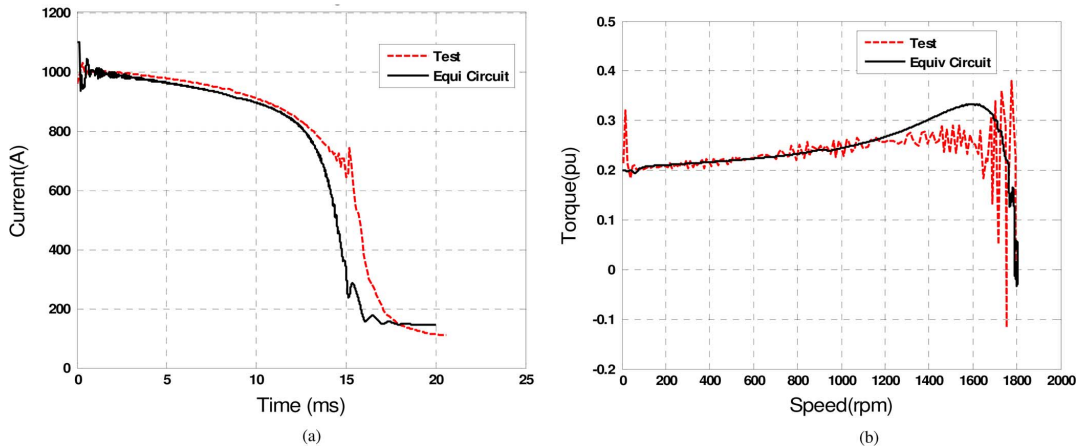


Fig. 7. Comparison of simulation and test results. (a) Simulated starting current I_n in comparison with test results. (b) Simulated accelerating torque in comparison with test results.

The resistances above are on the rotor side, or the secondary side. These rotor parameters should be transformed to the stator side, and the transformation can be expressed as

$$\begin{aligned} r'_{kd} &= \frac{(K_{dp1}W_1)^2}{(W_{kd})^2} \cdot \frac{r_{kd}}{s} \\ r'_{kq} &= \frac{(K_{dp1}W_1)^2}{(W_{kq})^2} \cdot \frac{r_{kq}}{s} \end{aligned} \quad (13)$$

where W_1 is the number of turns of the stator winding at d-axis; W_{kd} and W_{kq} are the number of turns of the rotor windings, and in this paper, their turns numbers of both virtual windings are set to be 1; and k_{dp1} is the stator winding factor.

The calculation of the leakage inductance is rather complicated with the analytical method because of saturation of the

pole tip. Fortunately, the leakage flux distribution and effects on the rotor inductance can be obtained through 2-D FEA. And it is shown that the influence of saturation on the rotor leakage inductance of the pole-tip saturation can not be neglected [28]. As discussed in the literature [28], the rotor leakage inductances, $L_{kd\sigma}$ and $L_{kq\sigma}$, can be calculated by using the finite element results. Since only 2-D static FEA is involved, the computation time is very short. In this paper, the 2-D FEA takes less than 2 min. These rotor leakage inductances should also be transformed to the stator side

$$\begin{aligned} L'_{kd\sigma} &= \frac{(K_{dp1}W_1)^2}{(W_{kd\sigma})^2} \cdot L_{kd\sigma} \\ L'_{kq\sigma} &= \frac{(K_{dp1}W_1)^2}{(W_{kq\sigma})^2} \cdot L_{kq\sigma}. \end{aligned} \quad (14)$$

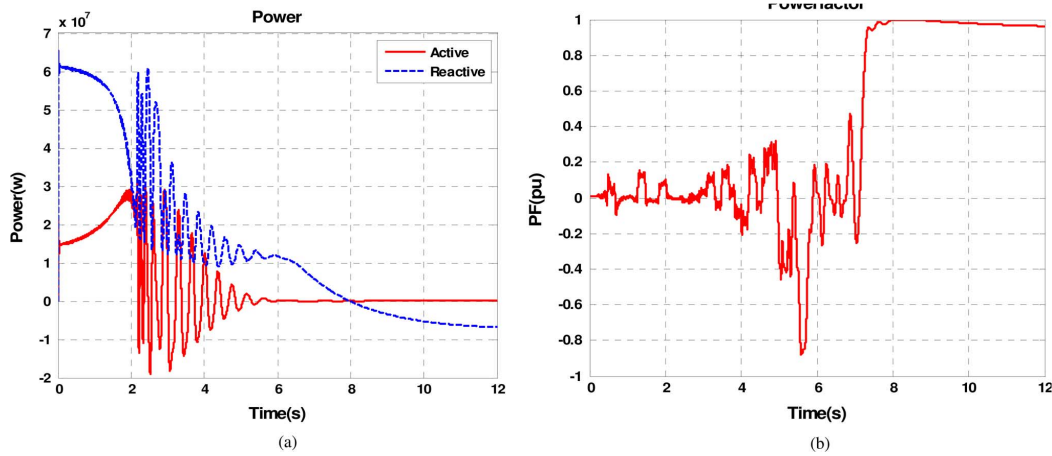


Fig. 8. Active, reactive and power factor during the starting obtained by equivalent circuit simulations. (a) Simulated input power during starting. (b) Simulated power factor during starting.

IV. SIMULATION OF STARTING PERFORMANCE

In order to validate the proposed model, the starting performance of the prototype SPSM was modeled using the proposed method, and compared with the test and 2-D transient FEM simulation [27]. In the test setup, the stator windings are supplied with half the rated voltage and the field winding is shorted through a discharge resistor to limit the induced currents of the field winding. The acceleration speed comparison between test, FEA and equivalent circuit model are shown in Fig. 4. It can be seen that the simulated result matches the test very well. But it should be noted that with transient 2-D FEA, it takes about 135 h of computing time. With the equivalent circuit model, it takes less than 2 min.

In this simulation, the rotor resistances vary with the rotor slip as shown in Fig. 5(a), where the resistance has been transformed to the stator side. The rotor leakage inductance along the d-axis is shown in Fig. 5(b). Conventionally, it is a function of flux density, but in Fig. 5(b) it is a function of the rotor current, which is suitable for this simulation.

Fig. 6 shows the flux and eddy current density distributions obtained from the 2-D transient FEA at rotor slip equal to 0.3. It can be clearly seen that the flux and eddy current are concentrated on the solid pole surface of the rotor, which indicates the significant skin effect during acceleration.

The starting current and torque are shown in Fig. 7. These waveforms show satisfactory agreement with test results. From the two-axis model, the active power, reactive power and power factor during the starting can be observed easily. These data are helpful to evaluate the stability and reliability of the power grid. Fig. 8 shows the simulated power waveforms. In this simulation, the rated voltage is applied to the motor.

It can be seen that because of the poor power factor during starting, a large amount of reactive power is needed. In this test setup, the total apparent power needed is 60 MVAR (or about five times of the rated power of the prototype). Therefore, the capability of the power grid should be taken into account for line-start applications of large SPSM. It can also be seen that after the dc voltage is applied to the field winding at near-synchronous speed, the power factor increases greatly as expected.

V. CONCLUSION

This paper presents an extended two-axis equivalent circuit model for the modeling of large solid pole synchronous motors with focuses on the starting performance simulation. The following can be concluded.

- With two set of separate virtual windings, the two-axis theory can be extended to the solid-pole synchronous motors.
- Skin effects must be taken into account in the rotor parameter calculations.
- This extended two-axis model can be used in both transient and steady-state simulations.
- The prohibitive CPU time needed to perform the simulation precludes the application of FEA in the calculation of starting performance of SPSM, especially at the early stage of the motor design iterations; and the extended two-axis model can save engineering time.
- Two-dimensional static FEA can be used to help the calculation of rotor leakage inductances to incorporate the influence of saturation during starting.
- The accuracy of the rotor parameters is critical. Variable rotor impedance that incorporates the skin effect with rotor slip improves the accuracy of the model.

All these conclusions have been validated by the test results on a 15 000 hp, 13.2 kV, four-pole solid-pole synchronous motor.

ACKNOWLEDGMENT

This work was supported by TECO-Westinghouse Motor Company. The authors thank Ansoft Corporation and Infolytica, Inc., for support in providing FEA software to the University of Michigan-Dearborn for this research.

REFERENCES

- [1] C. Concordia and H. Poritsky, "Synchronous machine with solid cylindrical rotor," *AIEE Trans.*, pp. 49–58, 1937.
- [2] C. T. Hsu, "Transient stability study of the large synchronous motors starting and operating for the isolated integrated steel-making facility," *IEEE Trans. Ind. Appl.*, vol. 39, no. 5, pp. 1436–1441, Sep./Oct. 2003.

- [3] M. J. Costello *et al.*, "Large synchronous motors for the Delaware city repowering project," *IEEE Trans. Ind. Appl.*, vol. 37, no. 5, pp. 1403–1412, Sep./Oct. 2001.
- [4] S. M. Silva, B. J. Cardoso Filho, M. G. Cardoso, and M. Rocha Braga, "Blower drive system based on synchronous motor with solid salient-pole rotor: Performance under starting and voltage sag conditions," *IEEE Trans. Ind. Appl.*, vol. 39, no. 5, pp. 1429–1435, 2003.
- [5] J. D. Park, C. Kalev, and H. F. Hofmann, "Analysis and reduction of time harmonic rotor loss in solid-rotor synchronous reluctance drive," *IEEE Trans. Power Electron.*, vol. 23, no. 2, pp. 985–992, Mar. 2008.
- [6] J. D. Park, C. Kalev, and H. F. Hofmann, "Modeling and control of solid-rotor synchronous reluctance machines based on rotor flux dynamics," *IEEE Trans. Magn.*, vol. 44, no. 12, pp. 4639–4647, Dec. 2008.
- [7] A. J. Wood and C. Concordia, "An analysis of solid rotor machines—Part IV," *AIEE Trans.*, pt. III, pp. 26–31, 1960.
- [8] C.-T. Hsu, H.-J. Chuang, and C.-S. Chen, "Power quality assessment of large motor starting and loading for the integrated steel-making cogeneration facility," *IEEE Trans. Ind. Appl.*, vol. 43, no. 2, pp. 395–402, Mar.–Apr. 2007.
- [9] H. Karmaker, "Practical design applications of time-stepping finite element analysis to salient-pole synchronous machines," in *Proc. IEEE PES Winter Meeting*, 2000.
- [10] T. W. Preston, M. A. Timothy, and A. M. Sitzia, "3-dimensional evaluation of the end parameters of large solid salient pole synchronous machines," in *Proc. 9th ICEMD*, Sep. 1–3, 1999, pp. 100–104.
- [11] S. Nabetta, A. Foglia, J. Coulomb, and G. Reyne, "A time-stepped finite-element simulation of a symmetrical short-circuit in a synchronous machine," *IEEE Trans. Magn.*, vol. 30, no. 5, p. 3683, Sep. 1994.
- [12] H. Yamada, "Pointing vector and impedance of solid pole synchronous motor by asynchronous operation," *IEEE Trans. Magn.*, vol. 17, no. 6, pp. 3247–3249, Nov. 1981.
- [13] S. Giurgea, H. S. Zire, and A. Miraoui, "Two-stage surrogate model for finite-element-based optimization of permanent-magnet synchronous motor," *IEEE Trans. Magn.*, vol. 43, no. 9, pp. 3607–3613, Sep. 2007.
- [14] G. R. Slemon, "An equivalent circuit approach to analysis of synchronous machine with saliency and saturation," *IEEE Trans. Energy Convers.*, vol. 5, pp. 538–545, Sep. 1990.
- [15] M. Chabane, B. Laporte, and F. Meibody Tabar, "Calculation of the performances of a synchronous machine with salient solid poles using the boundary integral method," in *Proc. 4th Int. Conf. Electrical Machines and Drives*, Sep. 13–15, 1989, pp. 43–47.
- [16] J. O. Ojo and T. A. Lipo, "An improved model for saturated salient pole synchronous motors," *IEEE Trans. Energy Convers.*, vol. 4, no. 1, pp. 135–142, Mar. 1989.
- [17] Y. Xiao, G. R. Stemon, and M. R. Iravani, "Implementation of an equivalent circuit approach to the analysis of synchronous machines," *IEEE Trans. Energy Convers.*, vol. 9, no. 4, pp. 717–723, 1994.
- [18] K. Shima *et al.*, "Steady-state magnetic circuit analysis of salient-pole synchronous machines considering cross-magnetization," *IEEE Trans. Energy Convers.*, vol. 18, no. 2, pp. 213–218, 2003.
- [19] M. Mirzaei, M. Mirsalim, and S. E. Abdollahi, "Analytical modeling of axial air gap solid rotor induction machines using a quasi-three-dimensional method," *IEEE Trans. Magn.*, vol. 43, no. 7, pp. 3237–3242, Jul. 2007.
- [20] J. W. Jansen, C. M. M. van Lierop, E. A. Lomonova, and A. J. A. Vandenput, "Modeling of magnetically levitated planar actuators with moving magnets," *IEEE Trans. Magn.*, vol. 43, no. 1, pp. 15–25, Jan. 2007.
- [21] D.-J. You, S.-M. Jang, J.-P. Lee, and T.-H. Sung, "Dynamic performance estimation of high-power FESS using the operating torque of a PM synchronous motor/generator," *IEEE Trans. Magn.*, vol. 44, no. 11, pp. 4155–4158, Nov. 2008.
- [22] W. Roshen, "Iron loss model for permanent-magnet synchronous motors," *IEEE Trans. Magn.*, vol. 43, no. 8, pp. 3428–3434, Aug. 2007.
- [23] H. E. Jordan, R. C. Zowarka, T. J. Hotz, and J. R. Uglum, "Induction motor performance testing with an inverter power supply: Part 1," *IEEE Trans. Magn.*, vol. 43, no. 1, pp. 242–245, Jan. 2007.
- [24] R. C. Zowarka, T. J. Hotz, J. R. Uglum, and H. E. Jordan, "Induction motor performance testing with an inverter power supply: Part 2," *IEEE Trans. Magn.*, vol. 43, no. 1, pp. 275–278, Jan. 2007.
- [25] A. J. Wood, "An analysis of solid rotor machines, part I, operational impedances and equivalent circuits," *AIEE Trans.*, pp. 1657–, 1959, Pt..
- [26] H. Karmaker and C. Mi, "Improving the starting performance of large salient-pole synchronous machines," *IEEE Trans. Magn.*, vol. 40, no. 4, pt. 1, pp. 1920–1928, Jul. 2004.
- [27] L. Luo, C. Mi, H. Karmaker, and P. Zhong, "Numerical modeling of large solid pole synchronous motors," in *Proc. ICEM 2006*, pp. 338–344.
- [28] K. Shima, K. Ide, and M. Takahashi, "Analysis of leakage flux distributions in a salient-pole synchronous machine using finite elements," *IEEE Trans. Energy Convers.*, vol. 18, no. 1, pp. 63–70, Mar. 2003.

Chunting Mi (S'00-A'01-M'01-SM'03) received the B.S.E.E. and M.S.E.E. degrees from Northwestern Polytechnical University, Xi'an, China, and the Ph.D. degree from the University of Toronto, Toronto, ON, Canada, all in electrical engineering.

He is an Associate Professor and Director of DTE Power Electronics and Electrical Drives Laboratory, University of Michigan, Dearborn. From 2000 to 2001, he was an Electrical Engineer with General Electric Canada, Inc. He was responsible for designing and developing large electric motors and generators up to 30 MW. He started his career at the Rare-Earth Permanent Magnet Machine Institute, Northwestern Polytechnical University. He joined Xi'an Petroleum Institute as an Associate Professor and Associate Chair of the Department of Automation in 1994. He was a Visiting Scientist at the University of Toronto, Toronto, ON, Canada, from 1996 to 1997. His research interests include electric drives, power electronics, electric machines, renewable energy systems, and electrical and hybrid vehicles. He has conducted extensive research and published more than 100 articles on the subject of electric machines, power electronics, and electric and hybrid vehicles.

Dr. Mi is the recipient of the "National Innovation Award," "Government Special Allowance Award," "Distinguished Teaching Award," and "Distinguished Research Award" of the University of Michigan, Dearborn. He is also a recipient of the 2007 IEEE Region 4 "Outstanding Engineer Award," "IEEE Southeastern Michigan Section Outstanding Professional Award," and the "SAE Environmental Excellence in Transportation (E2T) Award." He is the Chair of the IEEE Southeastern Michigan Section (2008–2009). He was Vice Chair of the Section from 2006 to 2007.

Yongbin Li received the B.S.E.E. and M.S.E.E. degrees from Shandong University, Shandong, China, and the Ph.D. degree from Shanghai University, Shanghai, China, all in electrical engineering.

He was an Associate Professor at Shandong University from 2000 to 2006. He was a Postdoctoral Researcher at the University of Michigan, Dearborn, from 2006 to 2007. He was a Research Assistant with Hong Kong University in 2005. Since the beginning of 2007, he has been a Technical Specialist with Johnson Electric Company, Hong Kong. He has extensive research on motor design and its drives, field analysis, and MCU control, and has published more than 30 articles in these areas.

Haran Karmaker (S'70-M'74-SM'82) received the B.Sc. Engg. degree from Bangladesh University of Engineering and Technology in 1967, and the M.A.Sc. and Ph.D. degrees from the University of Toronto, Toronto, ON, Canada, in 1971 and 1974, respectively, all in electrical engineering.

He joined the Engineering Laboratory, General Electric Canada, Peterborough, as a Research Engineer in 1975. Since 1981, he has been the Technical Leader of the Electromagnetics Team. He has led successful completion of many large collaborative research projects with Canadian and U.S. universities funded by GE, Canadian, and U.S. Governments. He has presented and published over 40 technical papers in IEEE, IEE, ICEM and other international journals. He is a co-author of the 2004 edition of *Handbook of Electric Motors* (New York: Marcel Dekker, 2004). His primary research activities include simulation and modeling of large rotating electrical machines, power electronic drives, and experimental studies for machine parameters, fields, and losses.

Dr. Karmaker has served IEEE Canada as Chair of Peterborough Section, Central Canada Council, Professional Development, and Educational Activities Committees. He is a Registered Professional Engineer in Ontario, a member of the IEC Technical Committees on Magnetic Steels and Rotating Machinery and the NEMA Rotating Electrical Machinery Committee. He has contributed to the development of IEEE, IEC, and NEMA standards. He is the current Chair of the Working Group on Revision of IEEE Standard 115 "Test Procedures for Synchronous Machines." In 1999, his team won the GE Industrial Systems Six Sigma Modeling Contest on Electrical Losses in Synchronous Machines.